Mean path length in refractive regular polygons and prisms

Matt Majic [*] and Walter R. C. Somerville [†]
MacDiarmid Institute for Advanced Materials and Nanotechnology, School of Chemical and Physical Sciences, Victoria University of Wellington, PO Box 600, Wellington 6140, New Zealand

(Received 2 November 2021; accepted 31 January 2022; published 22 February 2022)

We analytically derive the mean path length of light rays diffusely incident on refractive regular polygons of n sides (n-gons), analyzed from the dynamical billiards perspective and from ray optics. In polygons with sufficiently low refractive index, the mean path length is found to be equal to that in the invariant scattering case, i.e., the product of the mean chord length with the refractive index. If the refractive index is higher than some critical value, the mean path length is lower than the scattering value due to inaccessibility of trapped modes. Regular odd n-gons are found to have the same mean path length as $2n$-gons, when normalized against their mean chord length. There is a discontinuity between the mean path length in high n-gons and that in a circle, attributed to quasitrapped modes in high n-gons. This difference is removed with a small amount of absorption. We extend the results to refractive prisms with a regular polygon base, for example, hexagonal ice crystals. For prisms with any ergodic shaped base, we derive a simple formula for the mean path length.

DOI: 10.1103/PhysRevA.105.023518

I. INTRODUCTION

The absorption of light by a particle is a fundamental property pertaining to many areas of optics, including the studies of atmospheric aerosols and ice crystals, spectroscopy, optical cavities, and photovoltaic devices. Large weakly absorbing particles may be treated using the geometric optics regime where the absorption is derived from the path lengths of light rays incident on any object. For a nonrefractive object the mean path length reduces to the mean chord length, which depends only on the ratio of area to perimeter, due to the mean chord length theorem [1]. For a refractive material the mean path length is much more interesting. In particular, total internal reflection allows the possibility of trapped trajectories which reflect indefinitely at every interaction with the surface, which may be known as whispering gallery modes. These are typically studied in spheres, but have also been observed experimentally in hexagonal-based crystals [2], where rays are not strictly trapped.

The situation changes dramatically if we consider that all physical objects have imperfections which scatter rays randomly inside the medium. In this case the mean path length is simply related to the mean chord length by a factor of the refractive index (in two dimensions) or its square (in three dimensions), regardless of how quickly the light is scattered, so long as it is scattered at all [3,4]. However, physical objects also absorb light, and if the rate of scattering is insignificant compared to the rate of absorption, then the nonscattering mean path length is the relevant quantity (see [4], Supplemental Material IX). So here we study the nonscattering mean path length, but to do this we must consider the effect of scattering, together with concepts of dynamical billiards. A billiard is an idealized billiard table of any shape with a point billiard ball that reflects specularly, i.e., the angle of reflection equals the angle of incidence. Light rays in refracting objects are known as dielectric billiards [5] or open billiards [6], since if diffraction effects are negligible then rays reflect just like billiard balls but also have a probability of refracting out of the object. Billiard theory provides useful concepts and theorems from studying dielectric microcavities [7], which behave like dielectric billiards.

In this work we investigate the ray dynamics in regular polygons, regular polygon-based prisms, and prisms with irregular base shapes. In Sec. II we analytically calculate the mean path length in polygons. Section III considers ergodicity and its relationship to mean path length, and plots of phase portraits which encode the ray dynamics. Section IV discusses the effects of quasitrapped modes on mean path length. In Sec. V we consider absorption. In Sec. VI we derive the mean path length in polygon-based prisms. All results are checked against a customized R, C++ Monte Carlo ray tracing code on a standard desktop and the Rāpoi cluster.

II. MEAN PATH LENGTH IN A REGULAR POLYGON

Consider an n-sided regular polygon with a relative refractive index $s > 1$ to its surroundings, as shown in Fig. 1. The polygon is illuminated by diffuse lighting which corresponds to a Lambertian cosine distribution of rays externally incident at each surface point. A ray hits the surface at an angle θ_1, where it may either reflect back out or refract in and change angle according to Snell's law $\sin\theta_1 = s\sin\theta_2$, with probability given by the Fresnel coefficients. When the ray hits the surface from the inside it may reflect back in with the same angle, but it may only refract out if its angle to the normal is less than the critical angle of reflection $\theta_c = \mathrm{asin}(1/s)$; otherwise it undergoes total internal reflection. One may consider a simplified scenario where all probabilistic reflections are

[*] mattmajic@gmail.com
[†] wrcsomerville@gmail.com

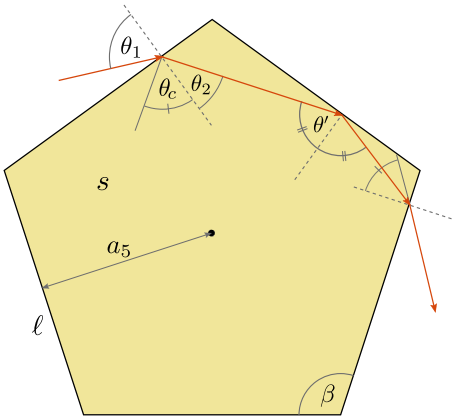

FIG. 1. Schematic of the system considered, for an example polygon with $n = 5$, edge length ℓ, apothem a_5, internal angle β, and relative refractive index s to its surroundings, which determines the critical angle of reflection θ_c. A representative example of a light ray refracts in from an angle θ_1 to θ_2, hitting an edge with $\theta' > \theta_c$ and therefore undergoing total internal reflection and then refracting out of the object due to hitting the surface with an angle less than θ_c.

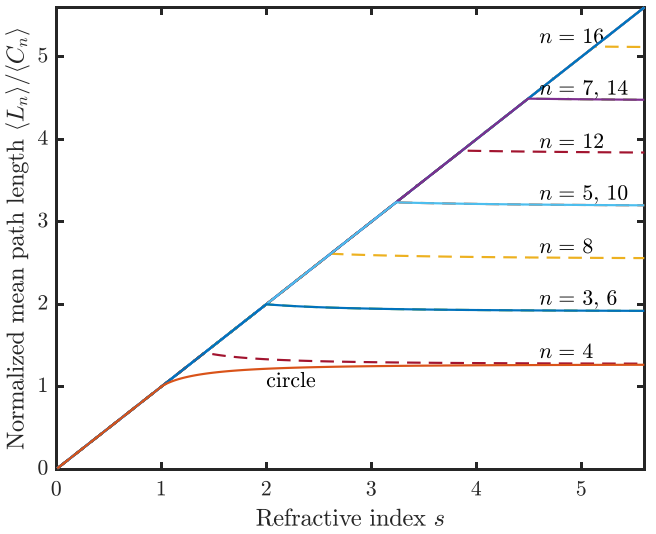

FIG. 2. Normalized mean path length of light rays in regular polygons with no scattering. Small values of n are shown, while $n = 9, 11, 13, 15$ and $n \geqslant 17$ lie entirely on the line $\langle L_n \rangle = s$ for the values of s shown.

replaced with refractions so that all external rays enter if they touch the surface and internal rays only reflect if $\theta > \theta_c$. This simplification does not affect the mean path length [4].

The direct approach to calculate the mean path length $\langle L \rangle$ would be to integrate the path lengths over all possible ray entry points and angles. However, rays may undergo total internal reflection multiple times, depending on their entry point and angle. Instead we will use a more nuanced approach, by comparison to the mean path length in the same object with scattering $\langle L_{\text{sca}} \rangle$. A simple model for scattering is to introduce a scattering coefficient that defines a finite probability per unit time that a ray will spontaneously change direction isotropically. When scattering is introduced the light rays will evenly fill the polygon both spatially and angularly, and this holds no matter how small the scattering coefficient, as argued in Appendix A. In two dimensions, $\langle L_{\text{sca}} \rangle$ has a simple formula independent of the scattering coefficient [3,4],

$$\langle L_{\text{sca}} \rangle = s \langle C \rangle = s\pi \frac{A}{P}, \tag{1}$$

where $\langle C \rangle$ is the mean chord length, A denotes the area, and P denotes the perimeter [8–10]. For regular polygons $\langle C_n \rangle = \pi a_n / 2$, where the apothem a_n is the distance from the center to the midpoint of a side. In special cases, $\langle L \rangle$ and $\langle L_{\text{sca}} \rangle$ are simply related by [4]

$$\langle L \rangle = P_E \langle L_{\text{sca}} \rangle, \tag{2}$$

where P_E is the probability that a scattered ray will escape the object without having to scatter again. Equation (2) only applies for objects where the internal spatial distribution of rays is uniform (without scattering). The distribution is in fact uniform regular polygons, which derives from a result in billiard theory [11] that for any closed polygonal billiard, almost every orbit (trajectory that reflects inside forever) fills the area uniformly. In an *open* billiard, the orbits eventually leave, but a diffuse distribution of rays will still fill the interior uniformly because of optical reciprocity: For any ray that leaves, there is another that enters at the same point and angle at the exterior (in the limit of an infinite number of rays) that continues the first ray's orbit inside the billiard. This uniformity is also confirmed by numerical simulations in Fig. 7.

Here P_E may be calculated as the fraction of scattering angles in $[0, 2\pi)$ that lead the ray to hit the surface with $\theta < \theta_c$ after any number of reflections. Heuristically, each side adds two escape wedges of angular width $2\theta_c$, rotated by π relative to each other, one corresponding to rays that refract out and the other for rays that refract in; by optical reciprocity, if a ray can enter, it can also leave. There are $2n$ escape wedges evenly spaced around $[0, 2\pi)$, but in even polygons, pairs of these wedges are identical. Defining $\bar{n} = n$ for n even and $\bar{n} = 2n$ for n odd, there are effectively $\bar{n}/2$ wedges with total angle $2\bar{n}\theta_c$, giving $P_E = \bar{n}\theta_c/\pi$. If s is low enough such that $\theta_c > \pi/\bar{n}$, then $\bar{n}\theta_c/\pi > 1$, which means rays cannot escape, but by reciprocity they cannot get trapped either. In this case we set $P_E = 1$.

Then Eq. (2) leads to the mean path length $\langle L_n \rangle$ of light rays inside an n-sided regular polygon:

$$\langle L_n \rangle = \begin{cases} \frac{\pi a_n s}{2} & \text{for } s \leqslant s_n = \frac{1}{\sin \frac{\pi}{\bar{n}}} \\ \frac{a_n s}{2} \bar{n} \theta_c & \text{for } s \geqslant s_n, \end{cases} \tag{3}$$

$$\bar{n} = \begin{cases} n & \text{for } n \text{ even} \\ 2n & \text{for } n \text{ odd.} \end{cases} \tag{4}$$

These are plotted in Fig. 2. The formula (3) agrees with Monte Carlo simulations of 10^7 rays to within accuracy of the standard deviation of five digits. For s lower than the critical refractive index s_n, we have $\langle L_n \rangle = \langle L_{\text{sca},n} \rangle$. For $s > s_n$, $\langle L_n \rangle$ decreases slightly with s and approaches $\bar{n} a_n / 2$. We have $\langle L_n \rangle < \langle L_{\text{sca},n} \rangle$ because a range of trajectory angles is only accessible with the addition of scattering. This is discussed in Sec. III.

A curious feature of Eq. (3) is the discontinuity at $n = \infty$ where the polygon tends to a circle of radius $a_\infty = a$. The

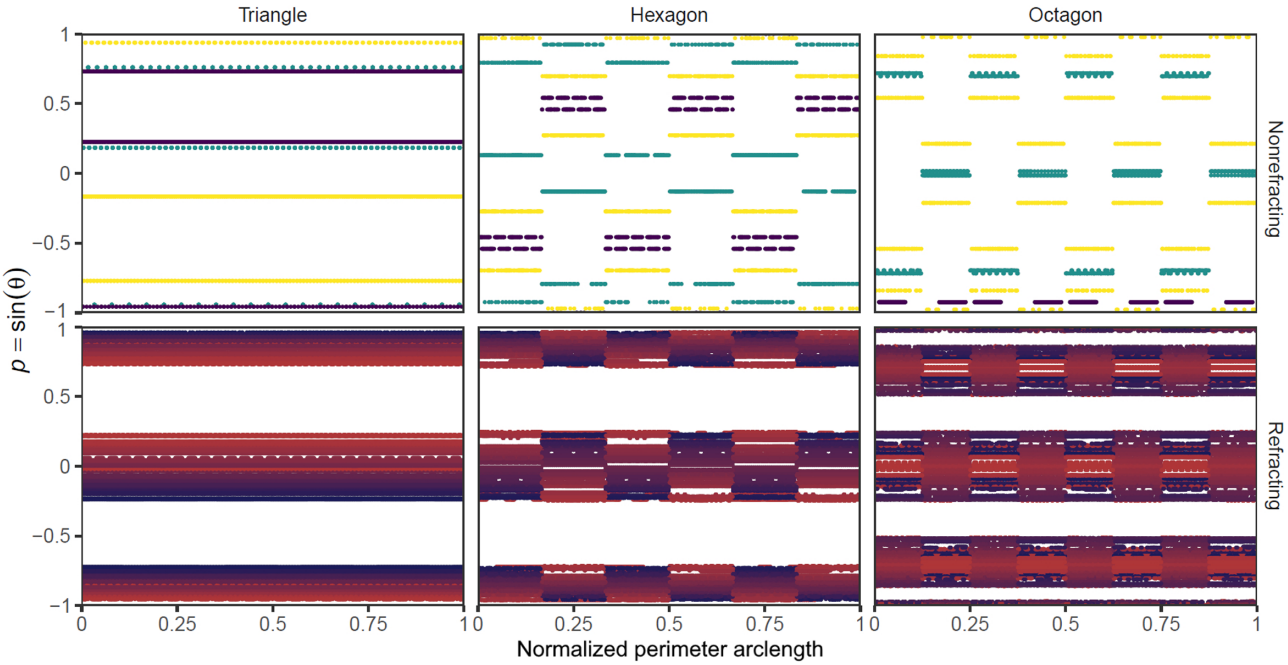

FIG. 3. Phase portraits of externally incident light rays on three polygons. The top panels are closed billiards where the first 1000 reflections of three random rays are shown, using one color for each ray. The bottom panels are open billiards with $s = 4$, where many random externally incident rays are shown, using one shade of color for each ray. The white gaps (trapped region) begin outward from $p = 1/s = 0.25$ for each polygon.

mean path length in the circle is [4]

$$\langle L_{\text{circle}} \rangle = a(s\theta_c + \cos\theta_c). \tag{5}$$

However, for an ∞-gon Eq. (3) gives $\langle L_\infty \rangle = \pi as/2$, which is significantly higher, as shown in Fig. 2. This discrepancy is due to quasitrapped modes as discussed in Sec. IV and is resolved by considering an infinitesimal absorption in Sec. V.

III. NONERGODICITY AND PHASE PORTRAITS

We should consider how the mean path length is related to ergodicity of the polygon when viewed as a closed billiard. For this we summarize some mathematical concepts of billiard theory [12–15].

The phase space of a billiard is the space of points on the perimeter and directions relative to the normal at each point. When a ray reflects inside the billiard it adds a point on the phase space at each reflection. An orbit is a trajectory extended infinitely forward and backward in time and fills countably many points on the phase space. A set of orbits occupies some measure (area) of the phase space. A billiard is ergodic if every set of orbits occupies either a measure of 0 (an infinitesimal area) or a measure of 1 (the entire phase space, possibly minus an infinitesimal area). Equivalently, a billiard is ergodic if almost all orbits explore the phase space uniformly densely. A regular polygon billiard is not ergodic because there are nonzero measure sets of orbits that omit some solid intervals in $[0, 2\pi)$ (shown in Fig. 3).

Nonergodic open billiards contain significant areas of orbits which may be confined to a region entirely outside the critical angle of reflection $|\sin\theta| > 1/s$. These orbits are infinite chains of total internal reflection. For diffuse external illumination these regions of the phase space will be empty, while the phase space is uniformly filled in the scattering case (see Appendix A), so we can deduce that $\langle L \rangle \leqslant \langle L_{\text{sca}} \rangle$. Ergodic billiards do not support any nonzero measure of trapped trajectories and the mean path length in ergodic shapes is unchanged by the addition of scattering, i.e., $\langle L \rangle = \langle L_{\text{sca}} \rangle$ for all s.

The top row of Fig. 3 plots three random orbits of the phase portraits of a closed triangle, hexagon, and octagon. In general, each orbit is restricted to a set of n horizontal lines, corresponding to the n angles that a ray acquires after many reflections. Almost any orbit will fill the boundary densely [16], but only strike the boundary with n angles. If n is odd or $n = 4$, the orbit fills the boundary completely with all n angles, but if n is even and $n \geqslant 6$, only half of the boundary is filled for each angle; rays never approach an edge with an angle that they would have reflected off at. This is seen in that the phase portraits are checkered. The square is an exception where a ray may hit the same face with opposing angles; the sharp angles between sides makes reversing direction within a small area ergonomically possible. The lower phase portraits in Fig. 3 are for a refractive index of $s = 4$, with many random externally incident rays. Nonergodicity is seen in that part of the phase space is empty; external rays cannot access some ranges of θ with $\theta > \theta_c$. The filled regions near $p = \pm 1$ correspond to total internal reflections of rays in free modes. The filled phase portraits for a triangle and hexagon are identical, due to the redundancy of opposing sides in scattering rays. The octagon portrait shows that as the number of sides increases, the trapped region splits into multiple regions, due to the

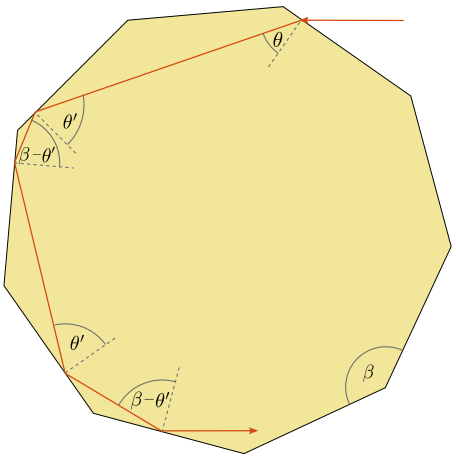

FIG. 4. Segment of a light ray reflecting and undergoing total internal reflection multiple times. Here β is the interedge angle, $\theta' = 2\pi(n/2-2)/n - \theta$, and $\theta < \theta_c$, while both $\theta' > \theta_c$ and $\beta - \theta' > \theta_c$.

increased range of angles generated by reflections. In contrast, irrational angled polygons are ergodic, for example the phase space of an irrational angled triangle is uniformly filled by one ray [17]. The phase portraits of polygons are very different to those of infinitely differentiable (smooth) billiards [18], where orbits are confined to either smooth curves or areas of chaos.

IV. QUASITRAPPED MODES

There are two types of long-lived modes in regular polygons: the strictly trapped orbits described in the preceding section, also known as whispering gallery modes, and quasitrapped modes, which are accessible from the outside and stay inside for a long time. These can occur in regular polygons with $n \geqslant 5$.

As shown schematically in Fig. 4, a ray may become trapped in a long cycle of total internal reflection if it refracts in at an angle θ such that it next reflects off an edge two edges along, at an angle $\theta' > \theta_c$, so that it undergoes total internal reflection, and then hits the next edge along. The next angle it makes is $\beta - \theta'$, where β is the internal angle between sides. If $\beta - \theta' > \theta_c$ and the ray keeps hitting sequentially adjacent edges, it will alternate between θ' and $\beta - \theta'$ and continually undergo total internal reflection until eventually it skips one too many edges and leaves. These are more prevalent if n is large, where rays do not have to cycle through strictly adjacent edges, while they cannot occur in triangles and squares since β is too small. These quasitrapped modes are what causes the mean path length in a high n-gon to differ from that in a circle.

In the phase portrait of the octagon in Fig. 3 (top right), the dark colored points represent a ray in a quasitrapped mode, which for 1000 bounces has managed to graze between sequentially adjacent edges (there are actually two closely spaced lines, one representing θ and the other $\beta - \theta$). The ray will eventually skip an edge and hit the boundary with a lower angle.

Figure 5 shows the number of rays that undergo a given number of total internal reflection events, taken from Monte Carlo data. The slope of the graphs is roughly $N \propto r^{-3}$ (where N is the number of rays and r is the number of reflections)

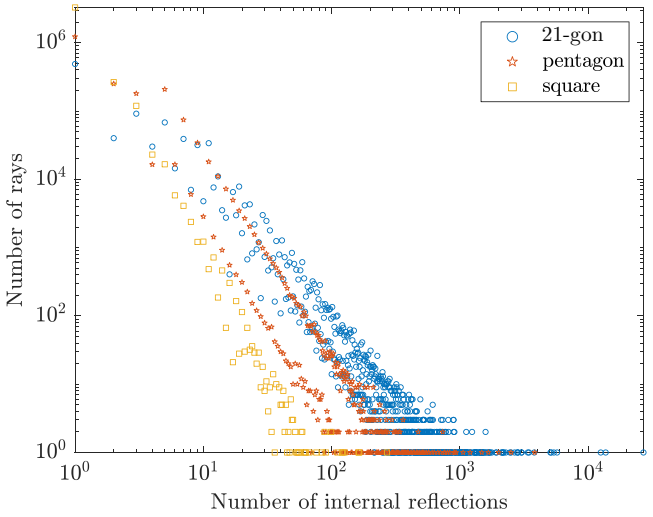

FIG. 5. Number of rays that experienced a certain number of internal reflections in a square, pentagon, and 21-gon with refractive index $s = 1.5$. Here 10^7 rays were used in each simulation. The highest number of recorded bounces was 270 in the square, ∼3800 in the pentagon, and ∼27 000 in the 21-gon.

and hence the average number of reflections is finite. The quasitrapped modes are represented in the tails of the graphs. These modes can be surprisingly long; our Monte Carlo simulation of 10×10^6 rays incident on a 51-sided polygon produced a ray that reflected 40×10^6 times. This makes numerical simulations for high-n-gons very noisy and billions of rays are required to calculate the mean path length accurately.

A peculiar feature seen in Fig. 5 is the bifurcation of reflection statistics, especially clear for $n = 5$. The lower split of the data represents even numbers of reflections, which means that rays are unlikely to undergo an even number of internal reflections. In fact, simulations showed that without probabilistic reflections, rays *never* reflect an even number of times in any regular polygon-shaped billiard.

V. ABSORPTION

We have seen that the mean path length in a high-n-gon differs significantly from that in a circle. In a physical scenario this will not necessarily be the case, because physical materials also absorb light. Of course there will also be scattering or surface imperfections, but as argued in [4] we may neglect scattering if it is insignificant compared to the rate of absorption. We introduce an absorption coefficient α which is a probability per short distance of a ray being absorbed by the medium. Another mechanism is tunneling through the boundary, even at angles corresponding to total internal reflection [5]; this could be modeled by a small probability of absorption per reflection. The exact mechanism does not affect the main results, so we will consider medium absorption.

The absorption of a sample illuminated by light rays with a path length distribution $p(L)$ is

$$A = 1 - \int_0^\infty e^{-\alpha L} p(L) dL, \tag{6}$$

and for $\alpha L \to 0$ the exponential may be replaced by its series expansion so that the fraction of rays absorbed A is propor-

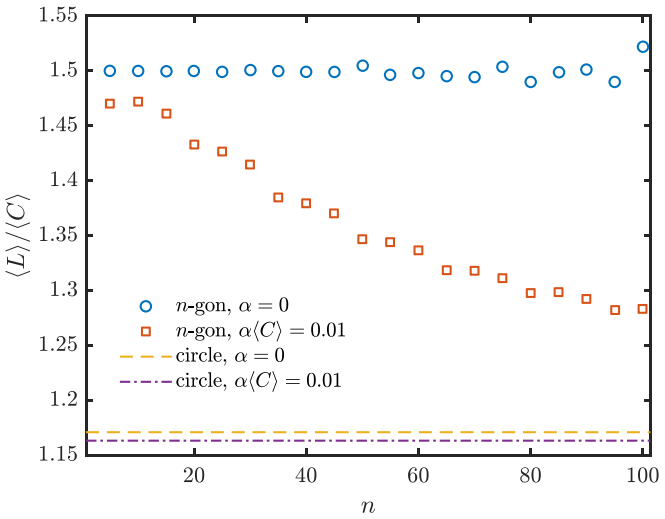

FIG. 6. Normalized mean path length in regular polygons with increasing number of sides, for glass with refractive index $s = 1.5$, with and without a small absorption of $\alpha\langle C\rangle = 0.01$. These are compared to the circle with and without absorption (which differ slightly, but this difference vanishes as $\alpha \to 0$). Here 10^9 rays were simulated for each n. For glass with a typical absorption coefficient of $\alpha \approx 1\ \mathrm{m}^{-1}$, $\alpha\langle C\rangle = 0.01$ corresponds to a diameter of about 12 cm.

tional to the mean path length:

$$A = \alpha\langle L\rangle + O((\alpha\langle L\rangle)^2). \tag{7}$$

This would imply that a high-n-gon absorbs more light than a circle, even as $n \to \infty$. However, the approximation (7) assumes that αL is small for all L where $p(L)$ has a significant contribution, i.e., that the absorption mean path length is much greater than the lengths of the ray paths. For a high-n-gon, quasitrapped modes are rare but long, such that they have a significant contribution to the mean path length. For $n \to \infty$, the vast majority of rays simply refract through with no total internal reflection just as they would in a circle, so the absorption A approaches that for a circle as $n \to \infty$, while the rare, would-be long modes get absorbed before making a significant contribution to the mean path length. This ability of absorption to quench the effects of small deviations in the boundary is similar to the effect that absorption has on small amounts of scattering [4]. Numerical simulations somewhat show this in Fig. 6, where for a small absorption of $\alpha = 0.01$ the general trend is $\langle L_{n\to\infty}\rangle \to \langle L_{\mathrm{circle}}\rangle$. Unfortunately, we could not compute $\langle L\rangle$ for $n > 100$ because the simulation time and statistical variance grow rapidly with n.

Figure 7 shows how a small absorption coefficient affects the spatial density in polygons. Without absorption, the ray density appears uniform (we did not have enough computation time to display the 100-gon without absorption, but it should be uniform). When absorption is added to the 20-gon and especially to the 100-gon, the ray density appears similar to that in the circle. We found that the internal density smoothly transitions from uniformity to that in a circle as either the absorption or number of sides increases. A similar aspect of absorption has been investigated in ergodic auditoriums, which are mathematically equivalent to closed billiards, with sound modeled as rays with a small probability of absorption at the boundary. There Ref. [10] draws a similar conclusion that the invariant mean path length $4V/\Sigma$ may be used to calculate the absorption only if the mixing rate of trajectories is sufficient compared to the absorption rate. Roughly speaking, the mixing rate is the rate at which trajectories are randomized over the phase space. The analog for our polygons is the rate that externally incident rays become randomly distributed over the area, which is slow for high-n-gons, and here the approximation (7) is invalid.

VI. PRISMS

We can extend our results for regular polygons to right prisms, made of a base shape extended perpendicularly (hence

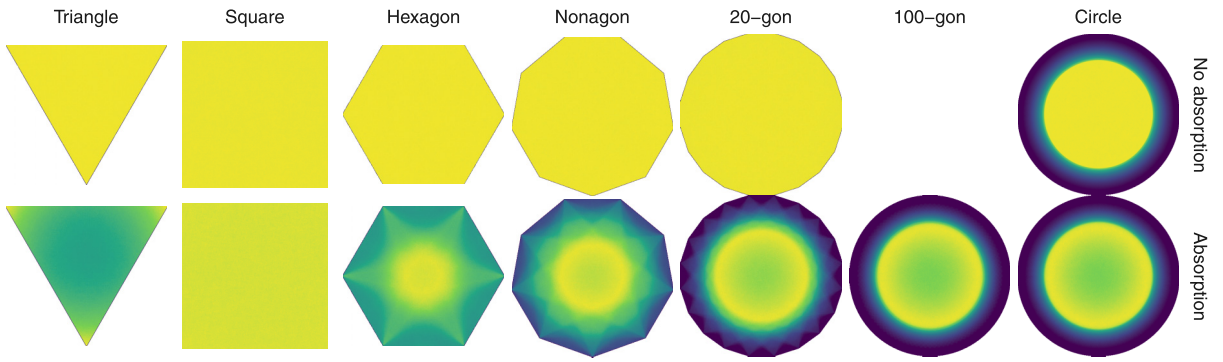

FIG. 7. Density of light rays from dark (low density) to light (high density). The polygons are made of glass with refractive index $s = 1.5$. The polygons in the top row do not absorb light, and this supports our statement that the density inside any sided regular polygon is uniform, even as the polygon approaches a circle, for which the density is nonuniform. In the bottom panels a reasonably small absorption is added, corresponding to the absorption of glass of roughly $\alpha \approx 1\ \mathrm{m}^{-1}$. The polygons are about 25 cm across, giving $\alpha\langle L\rangle \approx 0.25$, which is small enough to compare to the small-absorption limit. A rough indication of the absorption mean path is visible for the circle, which shows a slight decrease in intensity towards the center. The square appears uniform, but this depends on the absorption mean path. As the number of sides increases, the density exhibits more complex features but generally approaches that in a circle. The density in the 100-gon with absorption is indistinguishable from the circle, but we could not include a 100-gon in the nonabsorbing case due to extremely long trajectories causing issues with memory and time.

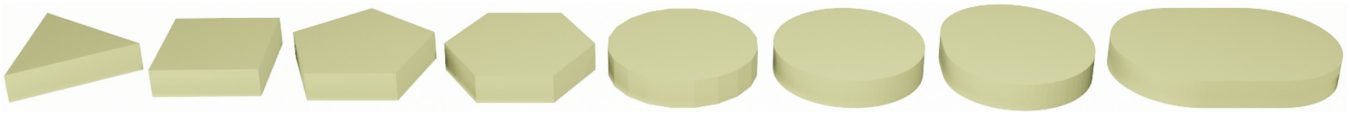

FIG. 8. Selection of prisms considered in this work, with bases from left to right: triangle, square, pentagon, hexagon, 20-gon, circle, limaçon, and stadium.

"right") a finite amount, as shown in Fig. 8. For any polygon-based prism, the mean path length may be calculated by assuming a uniform density of rays throughout the volume (we are not aware of a proof of this in three dimensions, but it appears true numerically) and using Eq. (2), $\langle L\rangle = P_E\langle L_{\rm sca}\rangle$. Actually, it will be easier to work with the probability of *trapping* from a scattering event, $P_T = 1 - P_E$. In the Supplemental Material of Ref. [4], P_T for a cube was expressed in terms of an integral over the spherical angles θ and ϕ about the normal of a chosen face that result in trapped trajectories. A cube is a square-based prism, and the geometrical derivations generalize straightforwardly to regular polygon-based prisms. Consider a ray that scatters at an angle θ to the vertical (the end faces are horizontal) and an angle ϕ about the vertical where $\theta = \pi/2$ and $\phi = 0$ point directly at a vertical face. We may restrict ourselves to $0 \leqslant \theta \leqslant \pi/2$ and $0 \leqslant \phi \leqslant \pi/m$ by symmetry and just consider reflection off the top and one vertical face (whose normal is $\phi = 0$ and $\theta = \pi/2$). For a fixed ϕ, the ray must have $\theta > \theta_c$ as to not escape out the top and $\theta' < \theta_c$ as to not escape out the vertical, where θ' is the angle to the normal of the vertical face, and one can show that $\cos\theta' = \sin\theta\cos\phi$. However, if $\phi < \phi_c$ where $\cos\phi_c = \cot\theta_c$, the ray is guaranteed to escape out the vertical side for any θ. Altogether, the probability of trapping is

$$P_T = \frac{\bar{n}}{\pi}\int_{\phi_c}^{\pi/\bar{n}}\int_{\theta_c}^{\sin^{-1}(\cos\theta_c/\cos\phi)} \sin\theta\, d\theta\, d\phi, \tag{8}$$

where again $\bar{n} = n$ for n even or $2n$ for n odd. The integral evaluates to

$$\begin{aligned} P_T = \frac{\bar{n}}{\pi}\mathrm{Re}\Bigg\{\sqrt{1-\frac{1}{s^2}}\Bigg[\sin^{-1}\left(\sqrt{s^2-1}\tan\frac{\pi}{\bar{n}}\right) \\ + \frac{\pi}{\bar{n}} - 2\cos^{-1}(\sqrt{s^2-1})\Bigg] - \sin^{-1}\left(s\sin\frac{\pi}{\bar{n}}\right) \\ + \sin^{-1}(s\sqrt{2-s^2})\Bigg\}. \end{aligned} \tag{9}$$

In three dimensions, the mean path length with scattering is $s^2\langle C\rangle$, so the mean path length in a regular n-gon-based prism is

$$\left\langle L_n^{\rm prism}\right\rangle = (1 - P_T)s^2\langle C\rangle, \tag{10}$$

where the mean chord length depends on the volume V and surface area Σ as

$$\langle C\rangle = 4\frac{V}{\Sigma} = \frac{2a_n h}{a_n + h} \tag{11}$$

for height h and base apothem a_n. One interesting feature is that P_T is purely a function of refractive index and the number of sides, independent of the object's height or base area. In other words, $\langle L\rangle/\langle C\rangle$ is independent of the prism's size or aspect ratio.

There are four piecewise components in the mean path length in Eq. (10). First, for $s \leqslant \sqrt{1+\cos^2(\pi/\bar{n})}$, the mean path is equal to that in the scattering case, because every trajectory is accessible from outside. For $s > \sqrt{1+\cos^2(\pi/\bar{n})}$ the mean path length is lower due the presence of trapped trajectories which spiral up and down the prism at a moderate angle, not too shallow or steep. There is another kink at $s = \sqrt{2}$ ($\theta_c = \pi/4$), because trapped trajectories suddenly no longer need to spiral; they can reflect with $\theta \gtrsim \pi/4$ between the ends and sides as in a rectangle. Finally, at $s = s_n = 1/\sin(\pi/\bar{n})$, the curve changes again because trapped trajectories now exist purely in the horizontal plane just as in the two-dimensional (2D) case. For the square-based prism, or cuboid, these last two conditions are identical. For triangular- and hexagonal-based prisms, the critical values are $s = \sqrt{7}/2 \approx 1.323$, $\sqrt{2}$, and 2, which are shown in Fig. 9(b). For pentagonal- and decagonal-based prisms, the values are $\sqrt{(13+\sqrt{5})/8} \approx 1.380$, $\sqrt{2}$, and $4/(\sqrt{5}-1) \approx 3.236$.

Just like the circle, a high-n-gon-based prism has a mean path length greater than the finite circular cylinder, which is derived in Appendix B to be

$$\langle L_{\rm cyl}\rangle = \begin{cases} \langle C_{\rm cyl}\rangle\left\{s^2(1-\cos\theta_c) + \frac{2}{\pi}[s\sqrt{s^2-1}\cos^{-1}(\sqrt{s^2-1}) + \cos^{-1}(s\sqrt{2-s^2})]\right\}, & 1 < s < \sqrt{2} \\ \langle C_{\rm cyl}\rangle[s^2(1-\cos\theta_c)+1], & s \geqslant \sqrt{2}, \end{cases} \tag{12}$$

where $\langle C_{\rm cyl}\rangle = 2ah/(a+h)$. This is also plotted in Fig. 9(a). Again, $\langle L_{\rm cyl}\rangle/\langle C_{\rm cyl}\rangle$ is independent of the aspect ratio.

As the number of sides of the base increases, the first critical value approaches $\sqrt{2}$ and the last critical value goes to infinity. For $n \to \infty$ it can be shown that $P_T \to \cos\theta_c - \sin\theta_c$ for $s > \sqrt{2}$, so the mean path length in a prism with a high-n-gon base is

$$\left\langle L_{n\to\infty}^{\rm prism}\right\rangle = \begin{cases} s^2\langle C\rangle, & s \leqslant \sqrt{2} \\ (1-\cos\theta_c+\sin\theta_c)s^2\langle C\rangle, & s > \sqrt{2}. \end{cases} \tag{13}$$

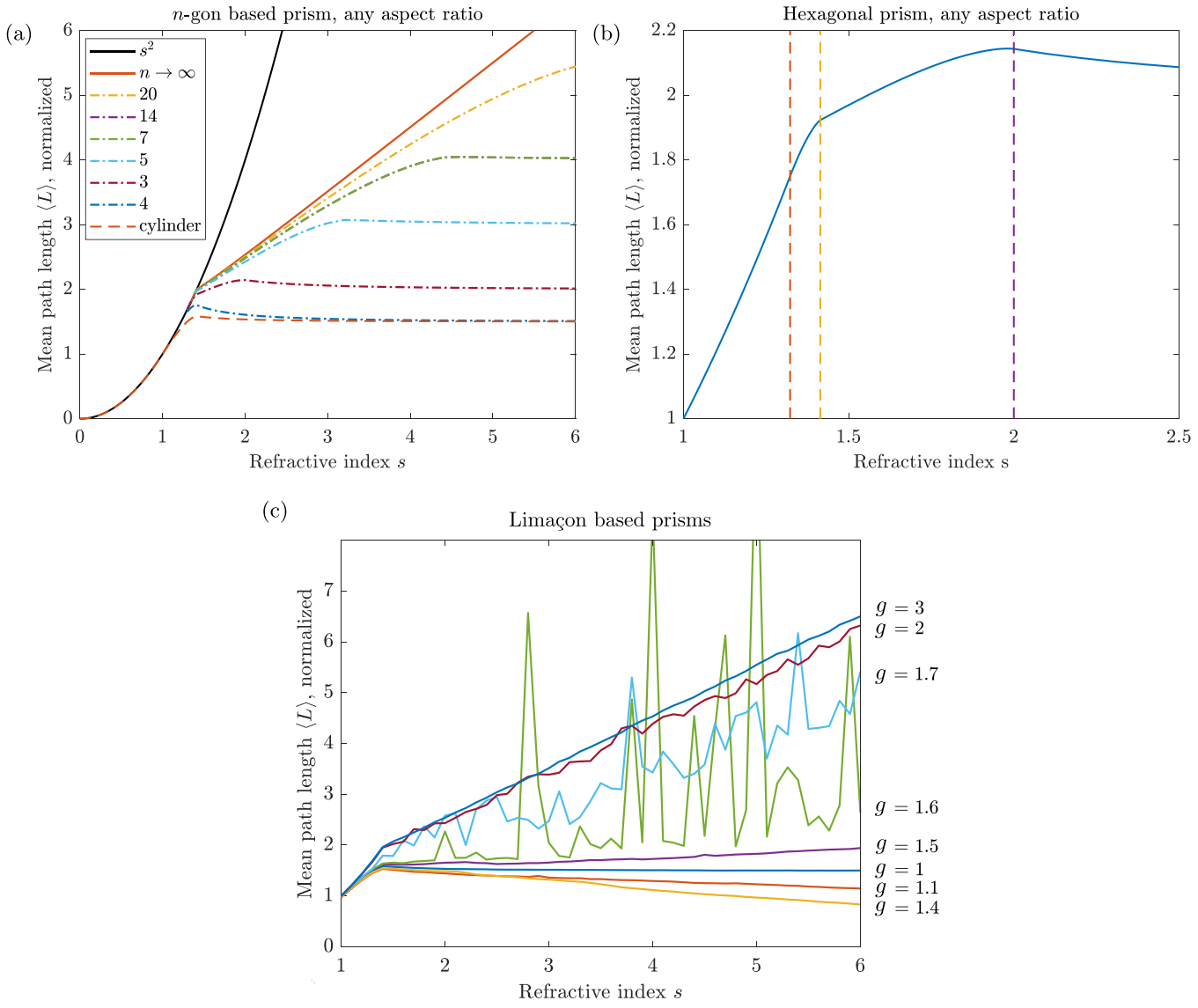

FIG. 9. (a) Mean path length for a variety of prisms, normalized such that $\langle C\rangle = 1$, plotted for high refractive indices to demonstrate the differences in the curves and test the formula (9) properly for the many sided cases. In the legend, s^2 is the mean path length with scattering, and $n \to \infty$ is calculated via Eq. (13). The curves for $n = 7$ and 14 overlap. Monte Carlo simulations with 10^8 rays agree with the analytic curves to within standard deviation, which is an absolute error ranging from approximately 10^{-3}–10^{-1} for $n = 14, 20$ to approximately 10^{-5}–10^{-3} otherwise, for all s shown. (b) Close-up of the mean path length in a refractive hexagonal-based prism of any aspect ratio, normalized by its mean chord length. The vertical lines are $s = \sqrt{7}/2, \sqrt{2}, 2$ from left to right, and mark discontinuities in the derivatives of the expression (9). (c) Mean path length in prisms with limaçon-shaped bases defined by $r = a + b\cos\theta$, with base "aspect ratio" parameter $g = (a + b)/(a - b)$. The limaçon stretches as g increases from $g = 1$ (circle) to 3 (the most deformed yet smooth and convex limaçon). For $g = 3$ the mean path length is indistinguishable from Eq. (13) and that of a stadium-based prism. The simulations were run with 10^{11} rays yet still produced noisy data for limaçons of intermediate aspect ratio, due to an extremely large statistical variance in the path lengths of individual rays.

This formula also applies to any prism with an ergodic base, and since ergodicity maximizes the mean path length, this makes $\langle L^{\text{prism}}_{n\to\infty}\rangle$ the upper bound for the mean path length in any prism where the top and bottom faces are perfectly parallel. In Fig. 9(c), Eq. (13) is checked against prisms with bases of a stadium and convex limaçons of varying eccentricity via Monte Carlo simulations of 10^{11} rays. The stadium is known to be ergodic [19] and its mean path length agrees with Eq. (13). The convex limaçon approaches ergodicity as it is deformed from the circle with increasing eccentricity, but is never completely ergodic; there are always small regions of stability [20–22]. Hence the mean path length in the limaçon prisms approaches Eq. (13) as the eccentricity increases. Interestingly, the mean path initially decreases with eccentricity, even though the phase space is more chaotic than in a circle; this may be due to decreased chord lengths of free modes. Figure 9(c) also shows that limaçon-based prisms of intermediate aspect ratio have a huge variation in ray path lengths. Of the 10^{11} incident rays, a very small number traveled enormous distances inside the prism and took *months* of

computing time to leave. So acquiring the mean path length in such nonabsorbing objects would require a different approach.

Orientation-averaged absorption of refractive particles may be calculated from the mean path length via Eq. (7), unless n is very large, as discussed earlier. Atmospheric hexagonal ice crystals have $s \approx 1.32 < \sqrt{7}/2$, so their absorption may simply be taken as $\alpha s^2 \langle C \rangle$. For most prisms here except the cuboid, the mean path length only decreases significantly from $s^2\langle C\rangle$ for $s > \sqrt{2}$. For cavities made of semiconductor materials with high refractive indices $s \approx 4$ [23], the mean path length differs significantly between the scattering and nonscattering cases and the mean path length could lie anywhere within these limits depending on the degree of imperfections.

VII. CONCLUSION AND OUTLOOK

We have investigated the mean path length in regular polygons and prisms, in relation to trapped modes and quasitrapped modes, and the link to concepts of ergodicity and phase portraits used in billiard theory. The existence of trapped modes was seen to decrease the mean path length compared to the scattering case as they are unpopulated without scattering and therefore the internal density is reduced, while quasitrapped modes increase mean path length as they are both long and accessible. We demonstrated the sensitivity of the mean path length to infinitesimal deviations in the shape boundary, in particular for a circle versus a regular polygon with an unbounded number of sides, and their corresponding prisms. We showed that this is reconciled in an experimental setting due to nonzero absorption that negates extremely-long-lived trajectories.

We have distinguished two types of whispering gallery modes which are an important ingredient for optical devices. Strictly trapped modes have been analyzed experimentally and theoretically also for diamond-shaped disks of sufficient refractive index [23]. We found quasitrapped modes in all polygons with five or more sides and their corresponding prisms, making these shapes candidates for optical resonators [2]. Our mean path length results provide an approximate absorption for atmospheric ice crystals [24–26]. Photovoltaic cells under diffuse or orientation-averaged illumination have upper bounds for mean path length and absorption in the slab geometry [27–29], but polygons with $n \geqslant 5$ have a wider range of path lengths than the slab due to whispering gallery modes; hence these geometries could be used to increase path lengths in photovoltaic devices. The results apply equally to high-frequency acoustic waves incident on objects of high impedance.

ACKNOWLEDGMENT

The authors are grateful to Eric Le Ru for useful discussions.

APPENDIX A: ISOTROPY IN OBJECTS WITH SCATTERING

It has been recognized numerically [4] and experimentally [3] that the mean path length of light in a convex refractive scattering object $\langle L_{\text{sca}} \rangle$ is independent of the medium scattering coefficient α_s. This was shown in [3] by assuming a diffuse distribution of rays throughout the object, but in the low scattering limit $\alpha_s \to 0$, diffusivity is not obvious due to the low population of rays traveling in trapped trajectories. Here will present a detailed argument that the internal distribution is actually diffuse for any α_s. We will consider 2D objects because of their connection to billiard theory, but the arguments extend naturally to three dimensions.

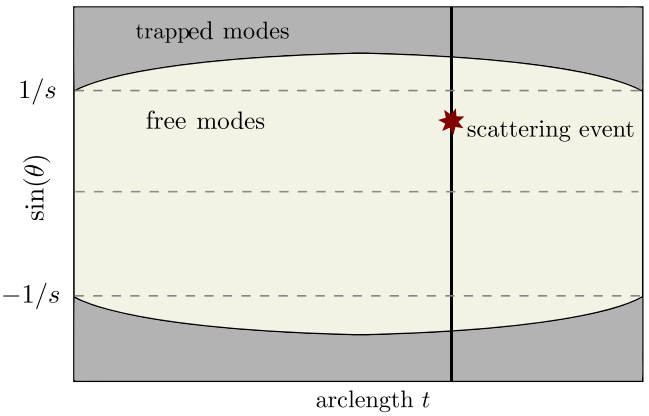

FIG. 10. Phase space of an arbitrary billiard with free modes in beige and trapped modes in dark gray. A scattering event occurs at the boundary where the ray may travel anywhere on the vertical line with equal probability.

First consider the object with no scattering: Rays refract in, may internally reflect a finite number of times, and refract out. In the phase space, rays incident from outside fill the middle strip with $|\sin\theta| < 1/s$ with a density of s relative to the exterior surroundings, due to the light focusing as it refracts into a denser medium. Areas with $|\sin\theta| \geqslant 1/s$ will be either empty or filled uniformly with the same density s because any area of the phase space is either completely hidden from or illuminated by internal rays with a density of s. At every point on the perimeter, there is a one-to-one correspondence between rays refracting in at some θ and rays about to refract out at $\theta + \pi$ due to optical reciprocity. This holds when the internal density is equal to s for all angles $|\sin\theta| < 1/s$, i.e., when the rates of influx and outflux are equal. So we may replace all refractions by reflections (the opposite of what we have done in the main text) and consider the object as a closed billiard.

1. Surface or boundary scattering

Now we add surface scattering. When a ray scatters it jumps to another point in the phase space with equal probability anywhere along the same vertical line, as shown in Fig. 10. This scattering transfers rays between the free and trapped subspaces, and the rate of transition of rays from each subspace is proportional to the area of each subspace, so the two will eventually equalize their densities. At the same time, the external flux from medium 1 holds the density of the free phase space uniformly at s, so ultimately the whole phase space gets filled with a density of s.

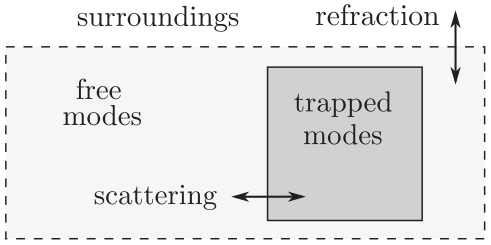

FIG. 11. Thermodynamic picture of ray scattering. The object (shaded) contains free modes, which are in thermal contact with the surroundings via refraction, and trapped modes, which are in thermal contact only with free modes via scattering.

It may help to think of the thermodynamic diagram in Fig. 11, where free modes are in thermal contact with a bath of rays in the surroundings (medium 1) and trapped modes are in contact with free modes via scattering. The trapped modes are in thermal equilibrium with the free modes, which in turn are in equilibrium with the surroundings.

2. Medium or internal scattering

In objects with scattering inside the medium, we can instead consider what may be called the "internal" phase space of points in the billiard table and directions of travel. For 2D billiards, the internal phase space has three dimensions, two spatial and one for ray direction. One dimension is redundant because rays travel in straight lines, so it is equivalent to the "boundary" phase space of the preceding section. Crucially, the boundary space is uniformly dense only when the internal space is uniformly dense and vice versa [1,8]. For the simplest case of isotropic scattering, when a ray scatters it jumps anywhere in a line of fixed position with equal probability. Then, just as argued for surface scattering, the trapped and free modes may exchange rays until the internal phase space becomes uniformly dense.

We can even consider a scattering phase function where a ray scatters at an angle θ relative to its initial direction, according to a probability distribution $g(\theta)$. If g satisfies detailed balance, meaning that repeated iterations of g lead to a uniform distribution in $[0, 2\pi)$, then this scattering has the same effect as isotropic scattering, only slower.

APPENDIX B: CALCULATION OF MEAN PATH LENGTH IN A FINITE CYLINDER

Here we outline the derivation of $\langle L_{\rm cyl}\rangle$ in Eq. (12) for a cylinder of tube radius a and height h. We calculate the mean path length as the weighted average (by area) of the mean path length of rays that enter the ends and the tube separately:

$$\langle L_{\rm cyl}\rangle = \frac{a\langle L_{\rm ends}\rangle + h\langle L_{\rm tube}\rangle}{a+h}. \tag{B1}$$

We will use two observations: Rays that enter the ends always leave through the other end if they have not already refracted out the tube and rays that enter the tube will always leave the tube if they have not already left through the ends. This makes the case $s > \sqrt{2}$ ($\theta_c < \pi/4$) straightforward because all rays that enter the sides cannot leave the tube (their angle of entry points too steeply down the tube) and vice versa; rays that enter the tube cannot leave the sides. So rays that enter the ends effectively experience the cylinder as an infinite slab; they have the same path length as if there were no tube (their paths may rotate about the vertical axis when reflecting off the tube but have the same path length). Then $\langle L_{\rm ends}\rangle = \langle L_{\rm slab}\rangle = 2hs^2(1-\cos\theta_c)$. Similarly, rays that enter the tube have a mean path length of that in an infinite cylinder: $\langle L_{\rm tube}\rangle = \langle L^{\infty}_{\rm cyl}\rangle = 2a$ [4]. Putting these into Eq. (B1) gives the bottom line of Eq. (12).

For $s \leqslant \sqrt{2}$, we assume that the ratio of mean path length to mean chord length is independent of aspect ratio, as it was for $s > \sqrt{2}$. So without loss of generality we may let the radius a of the cylinder go to infinity. Almost all rays that enter the ends will leave the other end without touching the tube, so again they have $\langle L_{\rm ends}\rangle = \langle L_{\rm slab}\rangle$. For $\langle L_{\rm tube}\rangle$, the tube makes up an infinitesimal fraction of the total surface area, so we may ignore the rays that refract out the ends as these only have finite path length. However, the rays that enter the tube and undergo total internal reflection off the ends cannot be ignored because they may have infinitely long path length. To calculate the mean path length of these rays, consider a right angle wedge between the top face and tube and let a ray enter the tube at an angle θ (post refraction) to the normal and ϕ about the normal ($\phi = 0$ points directly upward). Letting θ' be the angle that the ray makes with the normal of the top face, one can show that $\cos\theta' = \sin\theta\cos\phi$. Rays will reflect off the top if $\theta' > \theta_c$, which implies $\sin\theta < \cos\theta_c/\cos\phi$, but if $\phi > \phi_c = \cos^{-1}\cot\theta_c$, rays will reflect regardless of θ. If the rays reflect they will repeatedly do so and have a path length of that in an infinite cylinder, $L(\theta,\phi) = 2a\cos\theta/(1-\sin^2\theta\cos^2\phi)$ [4]. Altogether, the mean path length of rays that enter the tube is

$$\langle L_{\rm tube}\rangle = \frac{2}{\pi}\left\{\int_0^{\phi_c}\int_0^{\sin^{-1}(\cos\theta_c/\cos\phi)} + \int_{\phi_c}^{\pi/2}\int_0^{\theta_c}\right\} \times 2s^2\cos\theta\sin\theta\, L(\theta,\phi)\,d\theta\,d\phi, \tag{B2}$$

which can be evaluated using *Mathematica* to give the corresponding term in (12).

[1] R. Coleman, Random paths through convex bodies, J. Appl. Probab. **6**, 430 (1969).
[2] M. Grundmann and C. P. Dietrich, Whispering gallery modes in deformed hexagonal resonators, Phys. Status Solidi B **249**, 871 (2012).
[3] R. Savo, R. Pierrat, U. Najar, R. Carminati, S. Rotter, and S. Gigan, Observation of mean path length invariance in light-scattering media, Science **358**, 765 (2017).
[4] M. Majic, W. R. C. Somerville, and E. C. Le Ru, Mean path length inside nonscattering refractive objects, Phys. Rev. A **103**, L031502 (2021).
[5] H. E. Tureci, H. G. Schwefel, P. Jacquod, and A. D. Stone, Modes of wave-chaotic dielectric resonators, Prog. Opt. **47**, 75 (2005).
[6] E. Yablonovitch, Statistical ray optics, J. Opt. Soc. Am. **72**, 899 (1982).

[7] H. Cao and J. Wiersig, Dielectric microcavities: Model systems for wave chaos and non-Hermitian physics, Rev. Mod. Phys. **87**, 61 (2015).
[8] A. M. Kellerer, Considerations on the random traversal of convex bodies and solutions for general cylinders, Radiat. Res. **47**, 359 (1971).
[9] E. Czuber, Zur Theorie der Geometrischen Wahrscheinlihkeiten, Sitzungsber. Akad. Wiss. Wien **90**, 719 (1884).
[10] W. B. Joyce, Sabine's reverberation time and ergodic auditoriums, J. Acoust. Soc. Am. **58**, 643 (1975).
[11] C. Boldrighini, M. Keane, and F. Marchetti, Billiards in polygons, Ann. Probab. **6**, 532 (1978).
[12] N. Chernov and R. Markarian, *Introduction to the Ergodic Theory of Chaotic Billiards* (IMPA, Rio de Janeiro, 2003).
[13] S. Tabachnikov, *Geometry and Billiards* (American Mathematical Society, Providence, 2005), Vol. 30.
[14] J.-D. Polack, Playing billiards in the concert hall: The mathematical foundations of geometrical room acoustics, Appl. Acoust. **38**, 235 (1993).
[15] P. Richens and M. Berry, Pseudointegrable systems in classical and quantum mechanics, Physica D **2**, 495 (1981).
[16] W. A. Veech, Teichmüller curves in moduli space, Eisenstein series and an application to triangular billiards, Invent. Math. **97**, 553 (1989).
[17] R. Artuso, G. Casati, and I. Guarneri, Numerical study on ergodic properties of triangular billiards, Phys. Rev. E **55**, 6384 (1997).
[18] M. V. Berry, Regularity and chaos in classical mechanics, illustrated by three deformations of a circular 'billiard', Eur. J. Phys. **2**, 91 (1981).
[19] L. A. Bunimovich, On ergodic properties of certain billiards, Funct. Anal. Appl. **8**, 73 (1974).
[20] H. R. Dullin and A. Bäcker, About ergodicity in the family of limaçon billiards, Nonlinearity **14**, 1673 (2001).
[21] A. Bäcker and R. Schubert, Amplitude distribution of eigenfunctions in mixed systems, J. Phys. A: Math. Gen. **35**, 527 (2002).
[22] J.-B. Shim, A. Eberspächer, and J. Wiersig, Adiabatic formation of high-Q modes by suppression of chaotic diffusion in deformed microdiscs, New J. Phys. **15**, 113058 (2013).
[23] S. Shinohara, T. Harayama, T. Fukushima, M. Hentschel, T. Sasaki, and E. E. Narimanov, Chaos-Assisted Directional Light Emission from Microcavity Lasers, Phys. Rev. Lett. **104**, 163902 (2010).
[24] A. A. Kokhanovsky and A. Macke, Integral light-scattering and absorption characteristics of large, nonspherical particles, Appl. Opt. **36**, 8785 (1997).
[25] K.-N. Liou and P. Yang, *Light Scattering by Ice Crystals: Fundamentals and Applications* (Cambridge University Press, Cambridge, 2016).
[26] H. Lindqvist, J. Martikainen, J. Räbinä, A. Penttilä, and K. Muinonen, Ray optics for absorbing particles with application to ice crystals at near-infrared wavelengths, J. Quant. Spectrosc. Radiat. Transfer **217**, 329 (2018).
[27] R. Brendel, Coupling of light into mechanically textured silicon solar cells: A ray tracing study, Prog. Photovoltaics Res. Appl. **3**, 25 (1995).
[28] R. Mupparapu, K. Vynck, T. Svensson, M. Burresi, and D. S. Wiersma, Path length enhancement in disordered media for increased absorption, Opt. Express **23**, A1472 (2015).
[29] F. Tommasi, L. Fini, F. Martelli, and S. Cavalieri, Invariance property in scattering media and absorption, Opt. Commun. **458**, 124786 (2020).